Optical Fibre Pressure and Temperature Sensors for Minimal Invasive Diagnostics: Physiological Use

Beverley T Meggitt * : Sira Ltd, South Hill, Chislehurst, Kent BR7 5EH

Abstract

This paper describes a breadboard demonstrator optical fibre sensor system that was developed as a technology evaluator suitable for generic sensing applications. The system was based on a low-coherence interferometric processing scheme that utilised a capacitive feedback-controlled fibre coupled Fabry-Perot processing interferometer. Small size pressure and temperature sensing probes were constructed suitable for minimal invasive diagnostic applications including physiological use.

1. Introduction:

Many applications for optical fibre sensors require the use of miniature sensing probes in order to minimally disturb the measurement environment. One example of this need is in physiological use for the measurement of blood temperature, pressure and flow. It is also necessary for the sensor system to meet the requirement of resolution, dynamic range and long term stability amongst other criteria. Optical fibre low-coherence (or white-light) interferometry has the potential to meet the target requirements for such minimal invasive diagnostic use for both terrestrial and space applications. Here, work is described that resulted in the analysis, design and development of a demonstrator single mode optical fibre prototype sensor system based on the low-coherence interferometric technique and its evaluation in a testing programme over both a short and long duration periods. A common optical fibre based processing system was used for both pressure and temperature sensors demonstrating the suitability of the approach for a generic measurement technique.

2. Processing System:

The optical fibre sensor, low-coherence method has been undergoing a progression of recent developments since it has the capability of providing a high resolution over a large dynamic range without the need for a high degree of wavelength stability of the source as require by other interferometric methods e.g. pseudo-heterodyne technique. The sensor system approach adopted is illustrated in Fig 1. The processing interferometer and the sensor cavities were given a similar imbalance (~100 μm) and both set greater than the coherence length of the source used (~50 μm). A gain-guided 780 nm wavelength multimode laser diode operated below threshold was used as the broadband source and the optical processing interferometer used was of a bulk optic low-finesse Fabry-Perot form with one mirror scanned over $\lambda/2$ by a piezo-electric modulator in a saw-tooth waveform, Fig2(a) and 2(b). Previously work [1] has been reported using a Michelson interferometer feed-back controlled using a temperature stabilised reference sensor for a high temperature probe using multimode optical fibres. Here a modified commercially available optical fibre connected micro-filter [2] was used having low reflectance mirrors and operated in the transmission mode, representing the minimum possible configuration for the processing interferometer and therefore, potentially, the most stable [3]. The mean mirror separation and the linearity of the displacement ramp were capacitively sensed and stabilised via feed-back control to the piezo-electric element to 2 nm and 0.2% respectively. The fibre pigtailed source was current and temperature stabilised in order to give the required wavelength control of the source to <0.1 mA and 0.1^{o}C respectively.

* Present Address: Dept. of Electronic Eng., City University, Northampton Square, London EC1V OHB.

0-8194-1699-1/94/$6.00

3. Analysis:

An analysis was carried out of the Fabry-Perot processing interferometer and its performance was compared to that of the conventionally used Michelson interferometer in order to determine the relative signal to noise response of the two systems. For the case of the Fabry-Perot cavity operating in transmission, its transfer function can be shown to have the form:

$$I_t = I_O \frac{(1-R)}{(1+R)}\left[1+2\sum_{n=1}^{\infty} R^n \cos(n\phi_P)\right] \qquad [1]$$

where R is the mirror reflectivity, n the order of cavity reflection and ϕ_P is the optical phase.

For both the pressure and temperature sensor, a reflecting mirror was placed at a cavity length of 100 μm from the fibre end face. The diverging radiation reflected by the mirror resulted in a fraction G~0.015 of light being coupled back into the fibre along with the r~0.04 resulting from the silica/air interface at the fibre end, so forming the low finesse sensor cavity having a reflected intensity transfer function of:

$$I_r = I_o\left[r + G.(1-r)^2 + 2\sqrt{G.r}(1-r)\cos\phi_s\right] \qquad [2]$$

where ϕ_S is the optical phase of the sensor cavity. By avoiding use of lens elements, a low dimensional sensor was achieved. The output intensity function I_T is then given by:

$$I_T = \int (I_t.I_r).i(k)dk \qquad [3]$$

where i(k) is the (Gaussian) source spectral profile. Both the Fabry-Perot and the Michelson interferometers can be shown to have a similar output form of:

$$I_T = B_0 + B_1.\exp\left[-\left(\sigma(l_P-l_S)\right)^2\right].\cos\left[\omega t-2k_O(l_P-l_S)\right] \qquad [4]$$

where the exponential term represents the fringe visibility, ω is the induced carrier frequency, k_O the central wavenumber, l_P and l_S the optical cavity length of the processing and sensing cavities respectively and 2σ is the 1/e wavenumber spectral width. The coefficients B_O, B_1 for the Fabry Perot are given by:

$$B_0 = \frac{I_0}{4}\frac{(1-R)}{(1+R)}\left[r + G.(1-r)^2\right] \quad and \quad B_1 = \frac{I_0}{4}\frac{(1-R)}{(1+R)}\sqrt{G.r}(1-r).R \qquad [5]$$

and the corresponding signal/Shot-noise ($\propto B_1/\sqrt{B_0}$), shown in Fig 3 as function of R, is optimised for R=0.62. Comparison of the corresponding signal/Shot-noise (S/N_{Sh}) for the Michelson and Fabry-Perot processing interferometers can then be shown to have the form:

$$\frac{S/N_{Sh}\ \ Michelson}{S/N_{Sh}\ \ FabryPerot} = \frac{1}{2R}\left[\frac{(1+R)}{2(1-R)}\right]^{1/2} \qquad [6]$$

and for R=0.62 gives a relative $S/N_{Sh} \approx 1.2$. Therefore, the Fabry-Perot interferometer, while having a similar efficiency to the Michelson device, provides the potential for higher stability using capacitive feedback techniques.

3. Sensor Design:

Small sensing probes for monitoring temperature (10^oC to 50^oC) and pressure (0 to 200 torr) were constructed for concept evaluation with target resolutions of $1/10^oC$ and 1 torr respectively. For the temperature sensor the reflecting mirror (in the form of a short length of a silvered 600 μm diameter fibre stub) was set into one end of an aluminium tube ($\alpha=2x10^{-5}$), 0.8 mm in diameter into which the fibre was retrofitted as illustrated in Fig 4(a). Whereas the sensor cavity length was ~100 μm, the effective sensor length was much longer distance of $l_o=1$ cm in order to provide the necessary 0.01^oC resolution over a $\Delta T=40^oC$ temperature change (i.e. ~1^oC/fringe and 100 resolutions points/fringe). The sensor cavity length (the mirror-fibre separation) changes with temperature and was monitored by the corresponding phase changes induced in the output waveform of the processing interferometer. A cavity length change of 16 μm was produced for a 40^oC temperature change with a resolution of $<0.75^oC$. The change in cavity length Δl of the sensor is given by the relation $\Delta l = 2[l_o \alpha]\Delta T$.

The pressure sensor was based on a similar geometry of 1.8 mm diameter, 17 mm length with the fibre now deflected by a contacting flexible latex elliptical diaphragm (3:1 eccentricity) positioned in the *side* of the enclosing tube as shown in Fig 4(b). Pressure effects deflects the fibre (up to 0.8 mm) in a transverse arc motion across the reflecting end mirror with the central (elliptical) diaphragm deflection given by,

$$y = \frac{3P(m^2-1)b}{16m^2Et^3(6+4\alpha^2+6\alpha^4)} \qquad [7]$$

where P=applied pressure, m=(Poisson's ratio)$^{-1}$, t=diaphragm thickness (0.14 mm), E=Young's modulus, a and b the major and minor ellipse axes and $\alpha=b/a$. In doing so the cavity length of the sensor cavity is increased by up to 5 μm.. A cantilever effect (of length r=f+g; $\beta=f/g$ where f:g=13:4 mm) provides a mechanical advantage from the geometry used with the change in deflection of the fibre end given by $x=y.\beta$ and the resulting cavity length change predicted to have the form, $\Delta l = -r \pm \sqrt{(r^2+(y.\beta)^2)}$.

4. Digital Signal Processing:

The resulting serrodyne output fringe pattern from the sensor system was adjusted to give a single cosine fringe at a frequency of 25 Hz (300 Hz flyback frequency) equal to the ramp rate applied to the pzt element, Fig 2(a) and 2(b). In order to measure the phase and frequency of the waveform the fringe output was digitised using an ADC and then sorted in a computer data file. A curve fitting routine was then used based on a regression fit, to the general cosine form y = A + B.cos(C.x + D) where A,B,C and D represent the offset, cosine amplitude, cosine frequency (rad/sec) and phase angle (rad) to be determined. The curve fitting routine used was based on the cube-spline method from 64 data points taken over the ramp period and processed during the fast flyback.

5. Sensor Performance:

The temperature sensor was tested for response time, resolution, dynamic range and long term stability. The response time was performed by attaching the sensor to a small Peltier controlled aluminium platform that was temperature cycled in a sinusoidal fashion and 4000 data phase points taken over a 150 sec time period for 20 thermal cycles for a demand temperature amplitude of $\pm20^oC$. Fig 5 shows the monitored sensor response at a thermal frequency of 3 Hz. The sensor was able to followed the demand cycle up to a thermal slew rate of 4^oC/sec, limited by the processing bandwidth. The sensors were calibrated in a water bath against a Pt resistance thermometer showing a scale factor of 2^oC/fringe. The sensor resolution was determined to be 0.02^oC, limited by system noise.

The pressure sensor was calibrated at 20°C over a pressure range of 0 to 200 torr and measured against a precision pressure gauge (0.02 torr accuracy) utilising an internal reference quartz Bourdon tube. The time response, limited by the processing system, was equivalent to 2 fringes/sec. A non-linear pressure response was observed in optical phase change as shown in Fig 6, giving a maximum slew rate of 20 torr/fringe and a resolution of ~0.2 torr. The observed behaviour deviated from the anticipated quadratic form, attributed to the analytical model assumptions.

Acknowledgements: This work was carried out at Sira Ltd under ESTEC Contract No. 8043/88/NL/PB.

6. References:

1] Boheim, G: 'Remote displacement using a passive interferometer with fibre optic link': App. Opt. 24, 1985, p2335.

2] Queensgate Inst. Ltd microfilter 1990.

3] 'Minimal Invasive Diagnostics: Optical fibre sensors for temperature and pressure measurement': Vol 2, ESTEC Report, 1993.

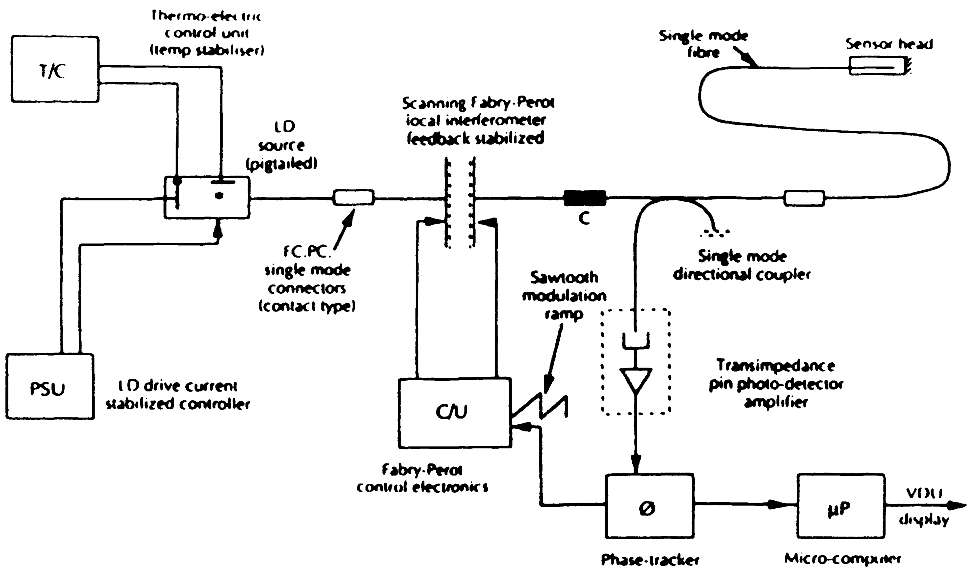

Fig 1.

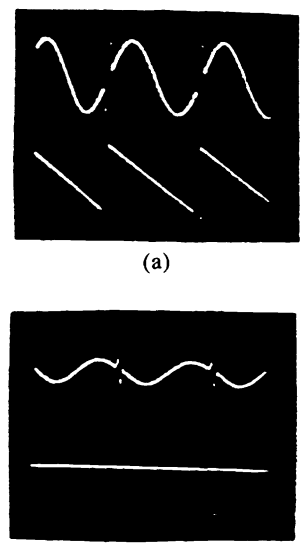

(b)
Fig 2.

Fig1: Schematic layout of demonstrator optical fibre sensor system.
Fig 2: (a) Cosine output waveform (upper) and sawtooth PZT drive (lower).
(b) Cosine output waveform showing modulation depth.

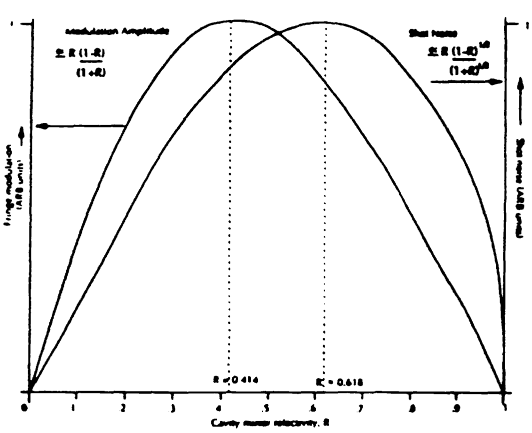

Fig 3. Signal/Shot-noise = f(R) - right curve/axis: Modulation depth = f(R) - left curve/axis showing optimum S/N_{Sh} @ R = 0.62 and maximum depth of modulation @ R = 0.41

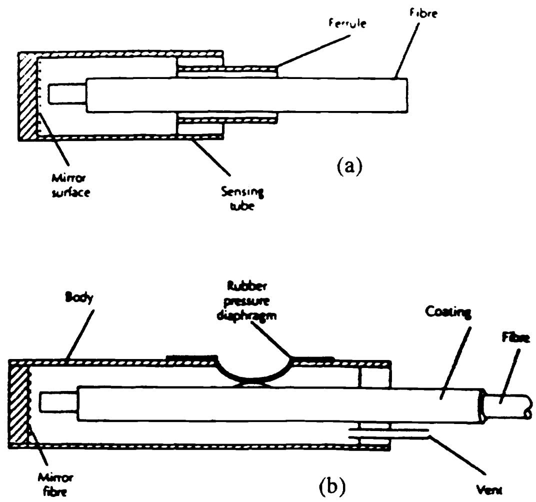

Fig 4. (a) Schematic of retrofitted temperature sensor probe: (b) Schematic of side diaphragm pressure sensor probe.

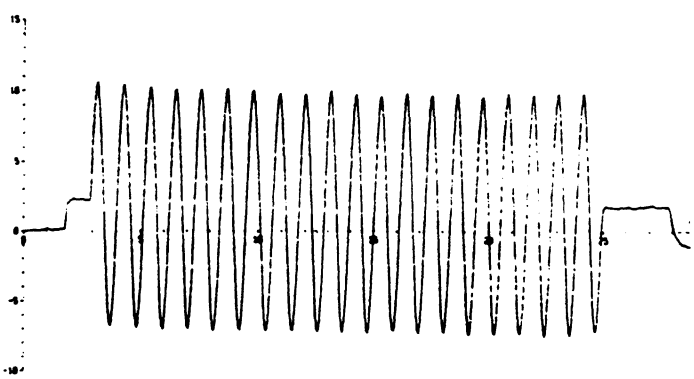

Fig 5. Temperature sensor output response to a ±20°C thermal cycle about 20°C at a 3Hz frequency.

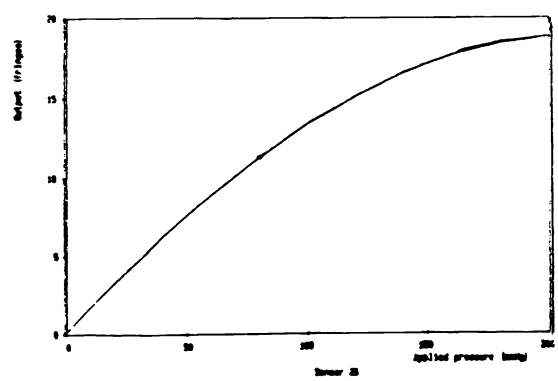

Fig 6. Pressure sensor response to a 0 - 200 torr pressure change (horizontal scale); 0 - 20 fringe (vertical scale) showing non-linear sensor characteristic.